2018 IEEE/RSJ International Conference on Intelligent Robots and Systems (IROS)
Madrid, Spain, October 1-5, 2018

Leg Design to Enable Dynamic Running and Climbing on BOBCAT

Max P. Austin, Jason M. Brown, Charles A. Young, and Jonathan E. Clark

***Abstract*— The design process for leg morphology has taken much of its inspiration from the manipulator community, including the concept of maximizing the workspace of a design. In this paper, we define the concept of Effective Dynamic Workspace, which examines the subset of the overall workspace capable of achieving the desired template dynamics. With this new design tool, the leg configuration of a new multi-modal platform BOBCAT is examined and refined. With the refined design, BOBCAT is able to achieve speeds of $2m/s$ while running and $0.17m/s$ while climbing a vertical wall.**

I. Introduction

Animals, such as cats, can run, jump, and even climb with a grace and agility that puts their current robotic counterparts to shame. Nevertheless, recent years have seen significant advances in the mobility of legged robots. A subset of these tasks, such as running [1]–[3], jumping [4], and climbing [5]–[7] can be performed dynamically, i.e. at animal-like speeds. Dynamic templates [8], such as SLIP [9], [10] and the pendular dynamic climbing model [5], [11], capture animals' center of mass dynamics and have been instrumental in designing and controlling these agile robots.

The most recent dynamic robots have an increased number of degrees of freedom in their leg designs, and consequently increased leg workspaces, which have enabled them to perform more than a single specialized task. Robots such as Cheetah [4] can both run and jump over obstacles and Minitaur [12] can run and bound up stairs. We have recently shown with SCARAB [13] that both the running and climbing templates can be instantiated on the same platform. For this robot, however, the transitions between modes required significant, manual changes to the legs.

In this paper we describe how the concept of an "Effective Dynamic Workspace" can be used to design the legs of our quadruped successor to SCARAB, Bobcat, to enable it to autonomously move in and translate between the dynamically distinct running and climbing modes. As a point of departure we start with the morphology defined by the dynamic quadruped Minitaur. Minitaur's directly driven 5-bar legs has two active DOF which has enabled us to get it to run at speeds of up to 3.0 m/s [14]. Although the workspace of the existing legs is large enough to allow it to adapt a flat posture suitable for climbing, the robot can not run up vertical walls.

Many robots, such as ANYmal [15], are designed to maximize the workspace of their legs. While helpful as a design tool for some tasks, it falls short for this dynamic, multi-modal scenario. For robot manipulators a variety of more restrictive workspace definitions have been introduced. Useful distinctions are made between the full "Reachable Workspace" and the more limited "Dexterous Workspace" (all points that can be reached with an arbitrary orientation). For mobile manipulators an "Effective workspace" is defined that excludes configurations that would cause the robot tip [16]. In the cable-driven robot community several definitions including "Dynamic Workspace" [17] or "Wrench-Feasible Workspace" [18] have been introduced. It is in the spirit of this class of workspace definitions, that we propose an "Effective Dynamic Workspace" (EDW) for legged robots. A robot has an EDW if the legs can generate the positions, forces, and velocities necessary for the desired dynamic motion. In our case this is the force and velocity profile of the feet necessary to achieve the template pendular climbing dynamics (described in Sec. II-A).

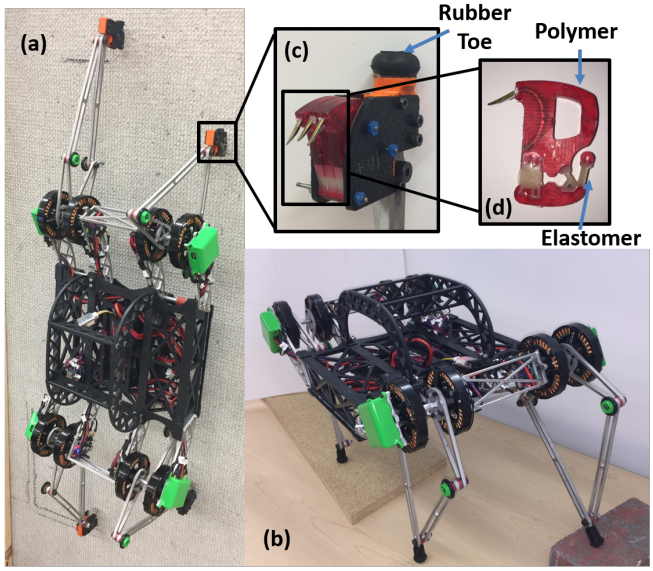

Fig. 1: BOBCAT platform in its standing configuration for climbing (a) and for running (b). The initial foot design to facilitate running and climbing (c) which has a rubber toe and holds the array of macrospines. Each macrospine (d) uses a hard polymer and elastomer for independent compliance.

In particular, we show how a leg linkage re-design using the Effective Dynamic Workspace as a guide enables our robot to achieve the necessary power to climb. We demonstrate this in the following manner: in section 2 we describe the calculations of both the kinematics and the force profiles associated with the effective dynamic workspace for dynamic climbing. Section 3 describes the construction of BOBCAT

FAMU/FSU College of Engineering, Tallahassee, FL 32310 email: jeclark@fsu.edu

(see Fig. 1) and its basic control strategy. The simulations and optimizations leading to the design of a linkage with an appropriate EDW are outlined in Section 4. Section 5 presents the empirical results of this new leg design on the running and climbing behavior of the robot. The paper concludes (Section 6) with a brief summary of the results and directions for future work.

II. Effective Dynamic Workspace

The concept of EDW is a metric to encode the necessary locomotion dynamics as constraints into the design process of limb morphology. By utilizing reduced order models, which have been shown to effectively capture the ground reaction force magnitudes and velocity profiles of both running and climbing animals, requisite force and foot velocity at each instant of a task can be determined. This extends the workspace constraints from considering just the static force or pose to include instantaneous power output constraints. These force and velocity constraints can then be mapped from the leg space to the motor space using varied kinematic configurations to examine the effect of linkage design for the defined task. Finally, since the template dynamics generally only capture the behavior within a single plane, additional constraints based on the out-of-plane dynamics are considered to ensure a feasible configuration.

A. Template Dynamics

Since Minitaur is already capable of high-speed running the focus of this study is on incorporating the climbing dynamics. The ground reaction forces and the center of mass profiles of climbing animals [11] and dynamic climbing bipedal [5], [6] and quadrupedal [13] robots have been shown to be captured by the Full-Goldman (FG) model. The model consists of a central mass supported by a linearly actuated arm in line with a linear spring pinned to the world frame at the foot. The model climbs by transitioning between two arms held at a fixed angular offset apart.

A modified version of the Full-Goldman model, Fig. 2a, was developed with a fixed linear offset between the legs rather than a fixed angular displacement to approximate the ground reaction forces for a multi-modal Minitaur-inspired platform. The point mass M is the full weight of the robot centered along the line between the front legs. The parameter k is the spring stiffness in line with the legs generated by the gains of the low impedance motors on the robot. The length L is prescribed to be to the linear retraction generated by the motion profile and D is half the body width of the robot. The angle of the arm θ with the vertical and the spring deflection s are determined through the dynamics.

$$\ddot{s}+\ddot{L}-\ddot{\theta}D=\dot{\theta}^2(s+L)-\frac{k}{M}s-g(\frac{s+L}{\sqrt{(s+L)^2+D^2}}-cos\theta) \quad (1)$$

$$\ddot{\theta}[(s+L)^2+D^2]+2\dot{\theta}(s+L)(\dot{s}+\dot{L})-2D(\ddot{s}+\ddot{L}) = -g(s+L)sin\theta+gDcos\theta \quad (2)$$

The equations of motion, Eq. 1 and Eq. 2, were derived using Lagrange techniques and can be used to compute the ground reaction forces in the plane of the wall during steady state running. The portion of the force profile within this plane is computed for a single step. For a quadruped trotting, the desired gait to be used while climbing, we assume the force to be evenly distributed between two stance legs.

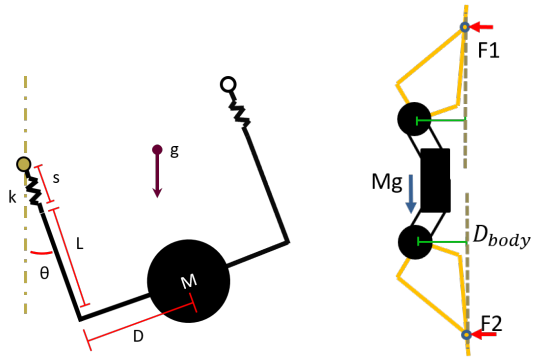

(a) Modified FG (b) Moment Model

Fig. 2: Force Models (a) Modified Full-Goldman model: The arm distance D and the spring stiffness k are held constant during a stride. The length L is prescribed. The spring deflection s and the body angle θ are determined from the equations of motion. (b) Free body diagram used to balance the moment.

Since the planar dynamic model does not consider the normal forces the robot will need to impart on the wall, this model is supplemented with a quasi-static model acting in the sagittal plane normal to the wall. The additional out of plane forces are computed via balancing the moment generated by the legs using the free body diagram shown in Fig. 2b. The distance D_{body} refers to the distance from the wall prescribed by the motion profile. M_g refers to the instantaneous force of gravity experienced by the robots center of mass based on the angle of the body θ from the modified FG. During steady state locomotion the pitching moment should be zero. Forces F_1 and F_2 represent forces that the robot must apply on the wall to counteract the pitch back moment induced by gravity. In general these forces are much smaller than the forces determined from the dynamic model. The lateral and sagittal forces on the foot are summed before mapping to motor space.

B. Kinematic Mapping to Motor Space

In order to convert the dynamic forces and motions from the foot into the motor space the kinematics of the generalized coaxial 5-bar (the general case of the symmetric coaxial 5-bar utilized on Minitaur [12]) are derived and shown in Fig. 3. The motor angles, M_1 and M_2, are measured globally from a horizontal line directly in front of the leg. The primary links L_1 and L_3 correspond to motor angles M_2 and M_1 respectively. The secondary linkages L_2 and L_4 connect to the primary linkages and are pinned to each other at the toe. These kinematics do not explicitly consider the toe extension which extends linearly from L_4 on the physical robot. The

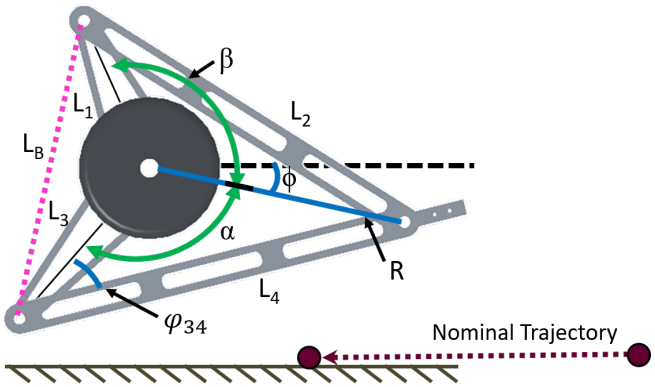

Fig. 3: Kinematic representation of the 5-bar linkage. The linkage lengths of the primary links which are connected to the motors are denoted by L_1 and L_3. The corresponding secondary linkage lengths are denoted by L_2 and L_4 respectively. The virtual leg length is R and the angle of the virtual leg is ϕ.

angles α and β relate to the angle of virtual leg ϕ such that:

$$M_1 = \alpha + \phi \tag{3}$$

$$M_2 = \beta - \phi \tag{4}$$

Unlike in the symmetric leg used on Minitaur, additional geometric constraints must be applied to ascertain the virtual leg length R and leg angle ϕ. L_B (the length between the knees), and ψ_{34} (the angle between L_3 and L_4) are defined by:

$$L_B = \sqrt{L_1^2 + L_3^2 - 2L_1L_3 * cos(M_{sum})} \tag{5}$$

$$\psi_{34} = cos^{-1}(\frac{L_B^2 + L_4^2 - L_2^2}{2L_4L_B}) \pm sin^{-1}(\frac{L_1}{L_B} * sin(M_{sum})) \tag{6}$$

$$M_{sum} = \begin{cases} M_1 + M_2, & \text{if knee down} \\ 2\pi - (M_1 + M_2), & \text{otherwise} \end{cases} \tag{7}$$

In the above equations linkage lengths are representing by the linkages' names. Given these added parameters, the angle α and the length of the virtual leg R were determined through the law of cosines, shown below.

$$R = \sqrt{L_3^2 + L_4^2 - 2L_3L_4 * cos(\psi_{34})} \tag{8}$$

$$\alpha = cos^{-1}(\frac{L_3^2 + R^2 - L_4^2}{2L_3R}) \tag{9}$$

From here the angle of the virtual leg ϕ is determined by inverting Eq. 3. The inverse kinematics can be found using the law of cosines from Eq. 9 (identically used to find β) which when combined with the known angle ϕ produce the motor angles M_1 and M_2 (Eq. 3 and Eq. 4).

$$J = \begin{bmatrix} \frac{\delta M_1}{\delta x} & \frac{\delta M_1}{\delta y} \\ \frac{\delta M_2}{\delta x} & \frac{\delta M_2}{\delta y} \end{bmatrix} = \begin{bmatrix} \frac{\delta \alpha}{\delta R}\frac{\delta R}{\delta x} + \frac{\delta \phi}{\delta x} & \frac{\delta \alpha}{\delta R}\frac{\delta R}{\delta y} + \frac{\delta \phi}{\delta y} \\ \frac{\delta \beta}{\delta R}\frac{\delta R}{\delta x} + \frac{\delta \phi}{\delta x} & \frac{\delta \beta}{\delta R}\frac{\delta R}{\delta y} + \frac{\delta \phi}{\delta y} \end{bmatrix} \tag{10}$$

The forces from the dynamic model are mapped to motor torques using the Jacobian of the generic 5-bar derived from the above kinematics.

C. Task Constraints

Additional constraints are applied in order to determine the position the leg takes in towards the wall to instantiate the climbing template dynamics. The constraints include ensuring attachment, minimizing the impact on out of plane dynamics, and balancing the pitch back moment. To ensure attachment, the foot space must be below the hip and be no shorter than inner primary link length, with the angle of the attachment mechanism constrained to be within a fixed angular deflection of vertical. To minimize the impact on the out of plane dynamics, the trajectory is set to be linearly retracting and maintains a fixed distance away from the wall throughout the stroke. The nominal offset distance D_{body}, shown in Fig. 2b, is set to the length of L_3 (the maximum length into the wall of the inner knee). This is held constant to regulate the pitch back moment created when the body mass is far away from the wall, and minimize the total amount of energy expended by regulating body distance from the wall. The maximum allowable extension is set to be slightly less than the maximum achievable kinematic length to avoid singularities. This extension is potentially larger than the allowable workspace so only the portion on the trajectory within the reachable space is considered for the motion profile.

The motion profile was constrained to have a minimum stroke length of $11cm$ which is necessary for the leg to properly recycle along its prescribed path during flight at high retraction speeds given the inertial load of the leg. The position of the robot body was also taken into consideration to ensure that the leg reaches further than robots frame which, when attached, is held closer to the wall than the central axis of the motors. The claws used to attach to the substrate require a certain range of angles in order to allow directional adhesion, therefore the angle L_4 makes with the wall must be computed. An allowable range of incident angles (determined via hand testing) was set to be between $+15°$ and $-10°$ from parallel. The sole constraint applied to the forces on the body is the maximum motor output from the linear motor model. In order to observe a larger space within the EDW additional trajectories were tested at both $+1$ and $+2cm$ closer to the wall and identically constrained.

III. BOBCAT Robotic Platform

With the goal of replacing SCARAB and achieving controllable multi-modal locomotion, the Minitaur platform was initially chosen as a starting point due to having legs with high speed and power with a reasonably large workspace [19]. The high power brushless DC motors which enabled the direct drive actuation are able to generate significantly more power than is required for steady state running, but initial tests to produce dynamic climbing resulted in failures. This motivated the design modifications described below.

A. BOBCAT Design

Fig. 1 shows BOBCAT with the 5-bar linkage morphology with coaxially-aligned motors used on Minitaur [12]. The following objectives guided the body design to better

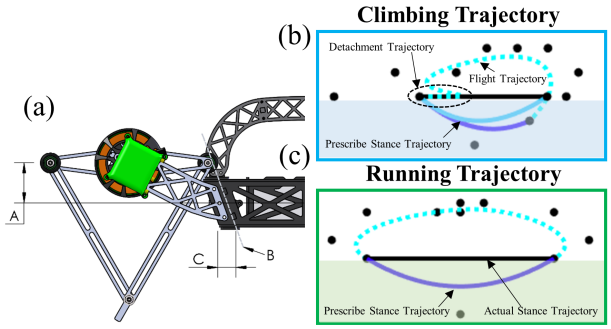

Fig. 4: a) The adaptation of the first generation Minitaur platform. The body structure was lowered 5.1cm with respect to the hips (A) to achieve a lower center of gravity. The fastening structure of the hips (B) is now oriented at an angle, which results in an additional 2.3cm of unimpeded leg-swing (C) within the workspace. b) Shows the climbing trajectory including the designed detachment phase at the beginning of flight c) The running trajectory implementing a simplified version of impulse control

facilitate climbing on BOBCAT: weight minimization, low the center of gravity (CG), and expansion the available workspace. The new ABS body structure and aluminum hip brackets of BOBCAT resulted in an overall mass, including the battery, of 5.0kg. The body and hip structures provide the necessary structural strength while relocating the body 51 mm lower relative to the hips (lowering the CG by 17 mm during standing). The unimpeded leg-workspace was extended 23mm towards the body, C in Fig. 4, through adaptation of the hip-to-body fastening interface. To maintain the direct drive capabilities, the motors, leg linkages, and related electronics were directly migrated from Minitaur to BOBCAT.

In order to improve the chances of successful attachment and prevent over penetration of the climbing substrate, arrays of independently sprung claws were developed based off of the microspine arrays used on robots such as BOB [14] and RiSE [20]. These toes shown in Fig. 1d, called macrospines, were similarly shaped to those used on BOB, with a springy tail and window to allow for constrained planar movement, however the thickness of each toe was increased to 4mm and stronger urethane rubber, 40A durometer, was used to generate the extension spring. The tensile strength of these macrospines was increases from its predecessor by over 16 fold, therefore a single toe is strong enough to support the robot's full weight. These were arranges into arrays of 3 toes per each ABS plastic foot.

B. Control

The controller implementation on BOBCAT leverages several of the benefits of direct drive actuation, namely tunable torsional spring stiffnesses and force approximation via motor effort, which have previously been implemented on Minitaur [19], [21]. Since BOBCAT is designed to generate multi-modal behaviors, the controller design was required to be able to operate both directly below the hips as well as almost directly in front of or behind the hips.

Previous running work on Minitaur implemented a smoothed feed-forward trajectory based around a reduced set of design points, [22], [23]. As such, a trajectory based approach with smooth foot paths generated via Bezier curves defined by the points on Fig. 4 (b) and (c) implementing a version of impulse control where the prescribed stance trajectory extends into the surface [24] was used for both running and climbing. Since running is primarily controlled in RP space, the torsional springs at the hips are transformed into a virtual prismatic and torsional spring pair via the manipulator Jacobian.

While the controllers for running and climbing are both implemented via a feed-forward trajectory, climbing has distinct trajectories for stance and flight, with the flight trajectory ending if stance is detected (when the position error in direction of the wall exceeds a hand tuned threshold). When stance is detected, the initial point of the stance trajectory is set to the current leg position while the terminal point remains fixed. The final nominal desired trajectory for both is shown in Fig. 4b and c. The nominal shape for the running behavior was designed to approach the teardrop shape implemented on Minitaur. The flight phase of the climbing controller was designed with a small upward extension vertically to improve detachment from the wall at the beginning of flight and a smooth approach into the wall that reaches into the wall until a maximum length is reached or until stance is detected.

Parameter	Value Range	Units
L_1	6-11	cm
L_2	15-25	cm
L_3	6-11	cm
L_4	15-25	cm
$\dot{L}$	70	cm/s
M	5	kg
k	1000	N/m

TABLE I: Parameters used in simulation sweep.

IV. Simulation for Leg Design

Solving for the motion and force profiles generated by the template dynamics of Sec. II, mapping those to a specific linkage configurations, and applying the motor limits filters away all possible linkages configurations which fail to possess a sufficient EDW. The viable designs are then refined and sorted by applying motor constraints, specifically peak torque and work ratio which will be described below. Finally an optimization of peak torques is used to select a single design.

A. Simulation Procedure

For this study, the task of climbing with the nominal speed of accession set to 70cm/s (corresponding to 1.5 body lengths per second [BL/s]), which is about as fast as DynoClimber, was chosen as a strenuous but realistic task for this platform.

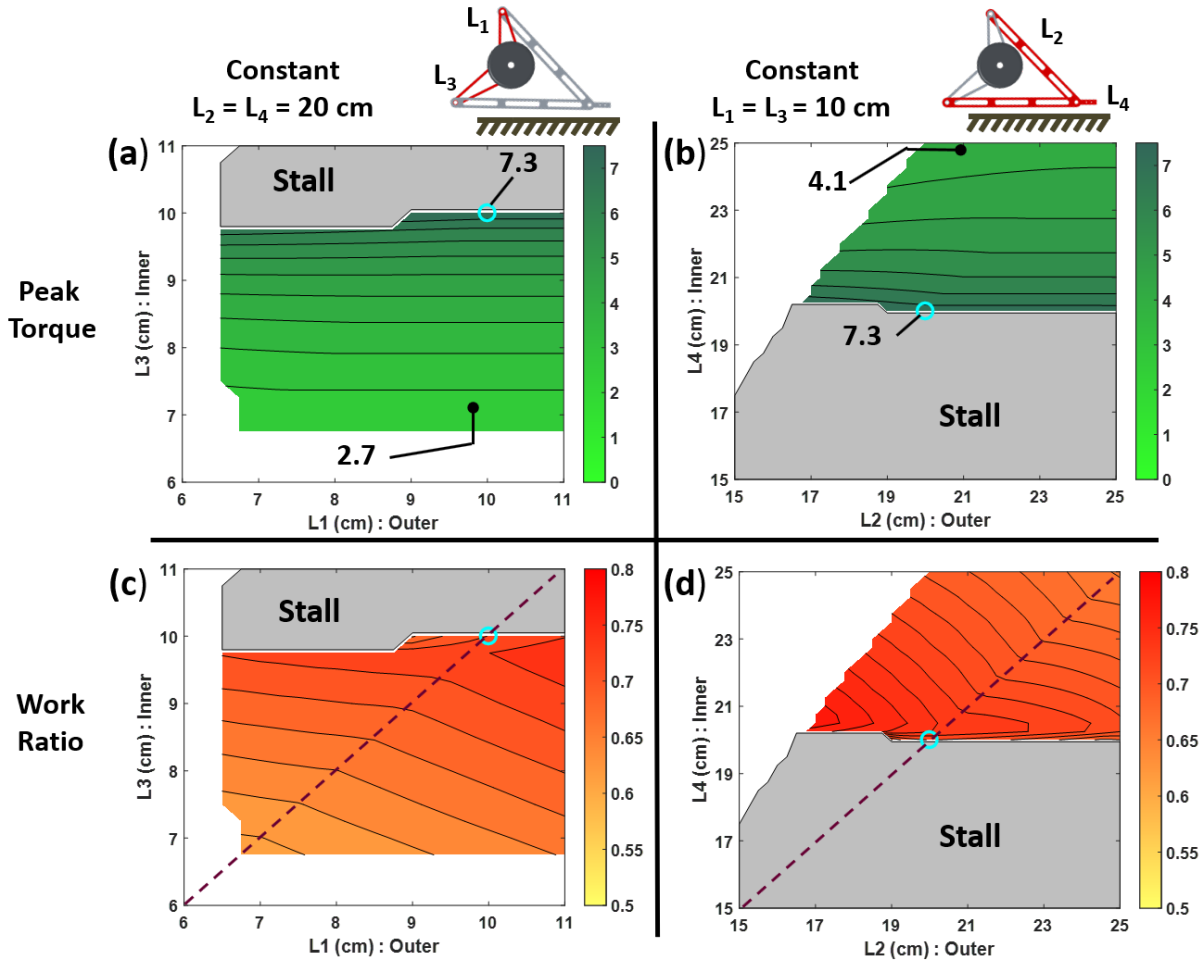

Fig. 5: 2D sweeps of linkage configuration holding linkages constant in the current configuration and sweeping the remaining two. (Left) Holding the primary linkages at a length of 10 and spanning secondary links (Right) holding the secondary linkages at a length of 20 and spanning primary links. Grey sections of the chart indicate a the range where a motor stalls. White sections indicate regions with insufficient stroke lengths.

The ranges of linkage lengths swept, shown in Table I, were defined around the initial symmetric design point with the primary links set to $10cm$ and the secondary links set to $20cm$. The lower bound of the primary links, L_1 and L_3, was set to maintain sufficient clearance with the motor radius while the upper bound is set only slightly larger than the nominal configuration as lengthening the moment arm would result in interference with the frame and surface. The secondary linkages were swept at lengths equal distances away from the nominal. All lengths were spanned in quarter centimeters increments to remain within reasonable manufacturing precision.

The force and trajectory from the dynamic template was mapped to the motor space using the kinematics defined in Sec. II-B and then further constrained to the motor model of the brushless U8 motor from T-motor ($\tau_{stall} = 7.5Nm$ and $\omega_{NL} = 84rad/s$) [25]. Once in the motor space, the peak torque of each motor (which is a primary limiting factor in achieving a desired behavior) and the work ratio, given by Eq. 11 [26] which is a measure of the balance in load distribution, are computed. Finally, the remaining linkage morphologies were sorted using Eq. 12 which determines the minimum average peak torque.

$$W_{ratio} = \frac{\dot{M}_1 \tau_1}{\dot{M}_1 \tau_1 + \dot{M}_2 \tau_2} \tag{11}$$

$$Cost = \frac{1}{\tau_{Pk1} + \tau_{Pk2}} \tag{12}$$

B. Simulation Results

Fig. 5 shows 2D cross sections of the set of viable designs (the 4 dimensional space of L1,L2,L3,L4), which were chosen to visualize the effect of link lengths on the performance criteria. Then from this space, the optimal design is determined using Eq. 12. Finally, the effective dynamic workspace is determined for the optimal and original linkage with both designs being experimentally tested.

1) Impact of Varying Primary Linkages: Examining the left column of Fig. 5 shows the impact of varying the primary linkages L1 (link away from the wall) and L3 (link in towards

the wall) from the current design point. Fig. 5a shows the peak torque in the motor has marginal correlation to changes in the outside primary link but significant correlation to changes in the inner primary link (which spanned a range of peak torque of $7.3Nm$ at a length of $10cm$ down to $2.7Nm$ at a length of $7cm$).

In terms of the entire 4-D workspace shortening the inner primary link to less than $7.25cm$ will prevent stall in all tested configurations, increased the success rate from only 15% at $11cm$, although it does not necessarily have a sufficient stroke length. Shortening the outer primary link however is only able to reduce stall marginally, increasing the number of successful cases by only 4%. Fig. 5c shows the work ratio's correlation to the primary linkages, which is generally decreased along the sets of symmetric links. However a greater number of striation are encountered along vertical variations, meaning the inner primary carries the greater influence over work ratio.

2) Impact of Varying Secondary Linkages: Examining the right column of Fig. 5 shows the impact of varying the secondary linkages L2 (link away from the wall) and L4 (link in towards the wall) from the current design point. Fig. 5b shows the peak torque has marginal correlation to changes in the outside secondary link (L2) but significant correlation to changes in the inner primary link (L4) (which spanned a range of peak torque of $7.3Nm$ at a length of $20cm$ down to $4.1Nm$ at a length of $25cm$).

In the 4-D space, lengthening the inner secondary link more than $24.5cm$ causes all linkages to avoid stall. Fig. 5d shows the work ratio's correlation to the secondary linkages, which is generally decreased along the sets of symmetric links. When the outer secondary link is longer than symmetry the work ratio becomes more heavily influenced by the inner secondary link and visa versa.

3) Optimal Configuration: The optimization converged to a leg with lengths $L_1 = 6.25cm$, $L_2 = 25cm$, $L_3 = 6.5cm$ and $L4 = 24.75$. The optimization converged to a region of the configuration space predicted by the 2D cross sections, with the primary links converging near the minimum allowable length and the secondary links extending to or near the maximum. Even though the outside linkages had marginal impact in the 2D sweeps, the optimum converged toward a near symmetric linkage, suggesting that as the various linkages change, the impact on these outside linkages increased. This near symmetric linkage reduced the work ratio to 53% from the nominal configurations work ratio of 73%. While the primary links converged close to the minimum bound, the optimum did not converge to the lower bound as the achievable stroke lengths would then be reduced.

C. Effective Dynamic Workspace Comparison

Fig. 6 shows the workspace of the nominal leg (left) compared with that of the optimum leg (right). The gradient corresponds to the maximum motor torque with a single leg supporting the full weight of the robot (worst case scenario) computed from the Jacobian. The nominal trajectory is shown in black. While the total workspace area of the optimum leg is 32% smaller, the Effective Dynamic Workspace is increased by 210%. The motors in the nominal configuration stall shortly into the trajectory while the optimum leg reduces the average requisite torque throughout the trajectory by more than half allowing it to achieve the full stroke within its kinematic limitations.

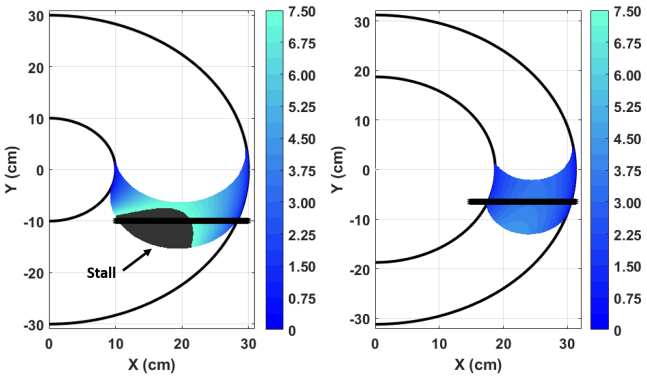

Fig. 6: The workspaces of a single leg for two configurations are presented here. A color gradient of the motor with the greatest torque under bodyweight loading is shown within the angles where successful attachment can occur. (left) the symmetric 5-bar used on minitaur, (right) the new 5-bar from the optimization

V. Experimental Validation

A. Experimental methods

In order to validate the design methodology, two distinct leg configurations (the nominal leg used on minitaur and a near optimal symmetric leg) were tested in both the horizontal and vertical domains. On board computing constraints limited the speed at which the kinematics of the asymmetric 5 bar could be computed, so only symmetric linkages were selected for experimental testing, with the resulting design point having $L_1 = L_3 = 6.5cm$ and $L_2 = L_4 = 25cm$. While this configuration's performance was not quite optimal, the change in peak torque is less than 2% from the optimal. The linkages were tested in both running and climbing where driving frequency of the leg is varied and the linear and torsional stiffnesses were held constant between leg morphologies. Speed and motor effort data were recorded during experimentation.

Climbing experiments were performed using the macrospines described in Sec. III-A attaching to a quarter inch wire mesh grid backed by carpet. Preliminary testing on a purely carpet wall resulted in inconsistent attachment, detachment, and more importantly, surface failures. The wire mesh grid was used to support the weight of the platform and thus reduce the chance for surface failures while still allowing for rapid attachment and detachment. In addition to the reinforced surface, the robot was constrained to out of plane direction using a nylon strap to regulate the out of plane

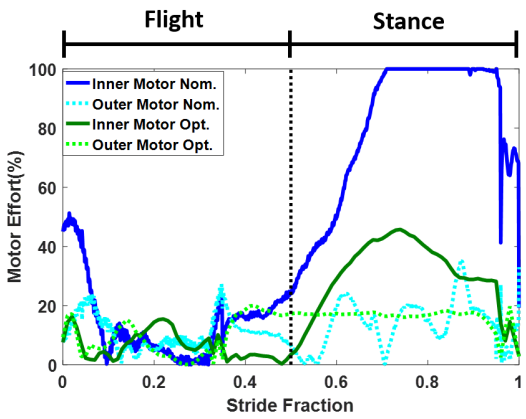

Fig. 7: Motor effort magnitude over an average stride while climbing for both the nominal linkage and the near optimal linkage morphologies.

dynamics which require precise tuning (which is outside the scope of this paper).

Running experiments were recorded using Vicon motion tracking system while climbing performance was measured using high speed camera footage. To ensure maximum power electrical power input, all experiments were run on battery which was kept above 95% of the maximum voltage.

B. Experimental Results

In climbing tests, the nominal 5-bar linkage morphology was incapable of climbing even with the constrained body dynamics. Motor effort for an average stride during a climb is shown in Fig. 7. The innermost motors of the nominal leg stalled mid-stride during any given test at both low and high driving frequencies, putting significant strain on the robots electronics and preventing completion of the stance trajectory. Using the near optimal leg morphology the robot was able to successfully climb unsupported at up to $3hz$. It was found that the innermost motor peaked at 49.4% of the full motor effort during climbing. During stance the average torque distribution between the motors is 56.99%. This matches similar data in simulation where the average work ratio for this linkage is 57%. Driving frequencies are limited to $3hz$ due to attachment issues with the substrate and inaccuracy of trajectory tracking without altering the stiffness of the virtual leg springs. The average climbing velocity at is approximately $17.5cm/s$ at this frequency.

BOBCAT showed comparable performance when running (see Table II) using both linkage sets. Both linkages were capable of traveling over $2m/s$ at driving frequencies from $5-7hz$. The peak velocity achieved was $2.3m/s$ using the near optimal linkage at $7hz$. The computed velocities using the nominal leg were slightly below that of the near optimal leg at all driving frequencies tested.

VI. Conclusion and Future Work

In this paper, a methodology for designing legged robots using a workspace based approach guided by template dynamics called the "Effective Dynamic Workspace" is demonstrated on a new robot BOBCAT. A new instantiation of the pendular dynamic climbing model is used to capture the desired template dynamics which is combined with a full set of constraints in both foot space and motor space (through the kinematics) to determine the effective dynamic workspace of a specific linkage.

Freq.	Optimal	Nominal
$5hz$	$2.0m/s$	$1.9m/s$
$6hz$	$2.1m/s$	$2.0m/s$
$7hz$	$2.3m/s$	$2.1m/s$

TABLE II: Running Performance of Both Linkages

The potential leg designs (a 4 dimensional space) was swept and the innermost linkages to the wall were found to have the greatest influence on the performance in terms of both average work distribution and peak torque while the outermost linkages only significantly impacted work distribution. An optimization was performed in order to determine linkages which best suit the task of climbing. This resulted in legs with shortened primary linkages and elongated secondary linkages. Although the total workspace was shrunk in the optimum linkage by 32% from the nominal configuration, the EDW of the leg more than doubled in size. Experimentally the robots was able to reduce the peak torque in climbing from a complete stall to just less than half of the motors max effort using the near optimum linage while maintaining running velocities over 2m/s.

In the future, we would like to expand the EDW design technique to incorporate several dynamic templates, specifically those needed to for full multi-modality which includes climbing, running, and jumping for dynamic transitions. Balancing the competing requirements for these distinct domains will require careful construction of constraints and optimization costs. Additionally, further development and tuning of BOBCAT will be required to negotiate the roll dynamics during climbing. With properly tuned controller for roll regulation BOBCAT should be able to freely perform running and climbing tasks at very low and high speeds.

Acknowledgments

This work was supported by the collaborative participation in the Robotics Consortium sponsored by the U.S. Army Research Laboratory under the Collaborative Technology Alliance Program, Cooperative Agreement DAAD 19-01-2-0012, and by NSF Grant CMMI-1351524. The U.S. Government is authorized to reproduce and distribute reprints for Government purposes not withstanding any copyright notation thereon.

References

[1] A. J. Ijspeert, "Central pattern generators for locomotion control in animals and robots: a review," *Neural Networks*, vol. 21, no. 4, pp. 642–653, 2008.

[2] S. Kim, J. E. Clark, and M. R. Cutkosky, "isprawl: Design and tuning for high-speed autonomous open-loop running," *The International Journal of Robotics Research*, vol. 25, no. 9, pp. 903–912, 2006.

[3] U. Saranli, M. Buehler, and D. E. Koditschek, "Rhex: A simple and highly mobile hexapod robot," *The International Journal of Robotics Research*, vol. 20, no. 7, pp. 616–631, 2001.

[4] H.-W. Park, P. M. Wensing, S. Kim *et al.*, "Online planning for autonomous running jumps over obstacles in high-speed quadrupeds," 2015.
[5] G. A. Lynch, J. E. Clark, P.-C. Lin, and D. E. Koditschek, "A bioinspired dynamical vertical climbing robot," *The International Journal of Robotics Research*, vol. 31, pp. 974–996, Apr. 2012.
[6] J. Dickson and J. Clark, "The effect of sprawl angle and wall inclination on a bipedal, dynamic climbing platform," in *International Conference on Climbing and Walking Robots and the Support Technologies for Mobile Machines (CLAWAR)*, 2012, pp. 459–66.
[7] B. D. Miller, P. R. Rivera, J. D. Dickson, and J. E. Clark, "Running up a wall: the role and challenges of dynamic climbing in enhancing multi-modal legged systems," *Bioinspiration & Biomimetics*, vol. 10, no. 2, p. 025005, 2015. [Online]. Available: http://stacks.iop.org/1748-3190/10/i=2/a=025005
[8] R. J. Full and D. E. Koditschek, "Templates and anchors: neuromechanical hypotheses of legged locomotion on land," *Journal of experimental biology*, vol. 202, no. 23, pp. 3325–3332, 1999.
[9] G. A. Cavagna, N. C. Heglund, and C. R. Taylor, "Mechanical work in terrestrial locomotion: two basic mechanisms for minimizing energy expenditure," *American Journal of Physiology-Regulatory, Integrative and Comparative Physiology*, vol. 233, no. 5, pp. R243–R261, 1977.
[10] R. Blickhan, "The spring-mass model for running and hopping," *Journal of biomechanics*, vol. 22, no. 11-12, pp. 1217–1227, 1989.
[11] D. I. Goldman, T. S. Chen, D. M. Dudek, and R. J. Full, "Dynamics of rapid vertical climbing in cockroaches reveals a template," *Journal of Experimental Biology*, vol. 209, no. 15, pp. 2990–3000, 2006.
[12] G. Kenneally, A. De, and D. E. Koditschek, "Design principles for a family of direct-drive legged robots," *IEEE Robotics and Automation Letters*, vol. 1, no. 2, pp. 900–907, July 2016.
[13] B. D. Miller and J. E. Clark, "Towards highly-tuned mobility in multiple domains with a dynamical legged platform," *Bioinspiration & biomimetics*, vol. 10, no. 4, p. 046001, 2015.
[14] J. Brown, M. Austin, B. Miller, and J. Clark, "Evidence for multiple dynamic climbing gait families," *Bioinspiration & Biomimetics*, vol. Under Review, 2018.
[15] M. Hutter, C. Gehring, D. Jud, A. Lauber, C. D. Bellicoso, V. Tsounis, J. Hwangbo, K. Bodie, P. Fankhauser, M. Bloesch *et al.*, "Anymal-a highly mobile and dynamic quadrupedal robot," in *Intelligent Robots and Systems (IROS), 2016 IEEE/RSJ International Conference on*. IEEE, 2016, pp. 38–44.
[16] Q. Huang, K. Tanie, and S. Sugano, "Coordinated motion planning for a mobile manipulator considering stability and manipulation," *The International Journal of Robotics Research*, vol. 19, no. 8, pp. 732–742, 2000.
[17] G. Barrette and C. M. Gosselin, "Determination of the dynamic workspace of cable-driven planar parallel mechanisms," *Journal of mechanical design*, vol. 127, no. 2, pp. 242–248, 2005.
[18] P. Bosscher, A. T. Riechel, and I. Ebert-Uphoff, "Wrench-feasible workspace generation for cable-driven robots," *IEEE Transactions on Robotics*, vol. 22, no. 5, pp. 890–902, 2006.
[19] G. Kenneally and D. E. Koditschek, "Leg design for energy management in an electromechanical robot," in *Intelligent Robots and Systems (IROS), 2015 IEEE/RSJ International Conference on*. IEEE, 2015, pp. 5712–5718.
[20] M. Spenko, G. C. Haynes, J. Saunders, M. R. Cutkosky, A. A. Rizzi, R. J. Full, and D. E. Koditschek, "Biologically inspired climbing with a hexapedal robot," *Journal of Field Robotics*, vol. 25, no. 4-5, pp. 223–242, 2008.
[21] D. J. Blackman, J. V. Nicholson, C. Ordonez, B. D. Miller, and J. E. Clark, "Gait development on minitaur, a direct drive quadrupedal robot," in *SPIE Defense+ Security*. International Society for Optics and Photonics, 2016, pp. 98 370I–98 370I.
[22] M. Austin, J. M. Brown, K. Geidel, W. Wang, and J. E. Clark, "Gait design and optimization for efficient running of a direct-drive quadrupedal robot," in *SPIE Defense+ Security*, 2017.
[23] J. Brown, C. Carbiener, J. Nicholson, N. Hemenway, J. Pusey, and J. Clark, "Fore-aft leg specialization controller for a dynamic quadruped," in *Robotics and Automation (ICRA) 2018 IEEE International Conference on*, 2018.
[24] D. J. Hyun, J. Lee, S. Park, and S. Kim, "Implementation of trot-to-gallop transition and subsequent gallop on the mit cheetah i," *The International Journal of Robotics Research*, vol. 35, no. 13, pp. 1627–1650, 2016.
[25] T-Motors, "U8 motor specifications," 2013.
[26] B. D. Miller, J. M. Brown, and J. E. Clark, "On prismatic and torsional actuation for running legged robots," in *Experimental Robotics*. Springer, 2016, pp. 17–31.